ACS OMEGA

http://pubs.acs.org/journal/acsodf

Article

Collaborative Enhancement of Humidity Sensing Performance by KCl-Doped CuO/SnO_2 p−n Heterostructures for Monitoring Human Activities

Lei Wang, Feng Huang, Xinqi Yao, Shuaishuai Yuan, Xinhai Yu,* Shan-Tung Tu, and Shijian Chen

Cite This: *ACS Omega* 2023, 8, 4878−4888

Read Online

ACCESS | Metrics & More | Article Recommendations | Supporting Information

ABSTRACT: In this study, a high-performance humidity sensor based on KCl-doped CuO/SnO_2 p−n heterostructures was fabricated by a ball milling−roasting method. The morphology and nanostructure of the fabricated KCl-CuO/SnO_2 composite were characterized by scanning electron microscopy, X-ray diffraction, transmission electron microscopy, X-ray photoelectron spectroscopy, and nitrogen sorption analysis. The results showed that the humidity sensor had a high sensitivity of 194 kΩ/%RH, short response and recovery times of 1.0 and 1.5 s, a low hysteresis value, and good repeatability. The energy band structure and complex impedance spectrum of the KCl-CuO/SnO_2 composite indicated that the excellent humidity sensing performance originated from the ionic conductivity of KCl, the formation of heterojunctions, the change in the Schottky barrier height, and the depletion of electronic depletion layers. The KCl-CuO/SnO_2 sensor has great potential in respiratory monitoring, noncontact sensing of finger moisture, and environmental monitoring.

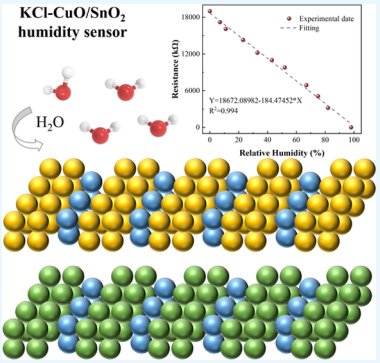

1. INTRODUCTION

In recent decades, wide-ranging and intensive research has been focused on the control of environmental humidity in industry, agriculture, and medicine. Precise and stable humidity sensing is important for monitoring instrument corrosion,[1] leakage of high-temperature vapors,[2] agricultural cultivation,[3] and human respiration.[4−6] Fabrication of humidity sensors featuring high sensitivities, low hysteresis, fast responses, short recovery times, and strong stabilities is currently the main challenge.[7]

Resistance and capacitance humidity sensors have become important research goals due to their simple structures and easily industrialized production. Unquestionably, sensitive materials directly affect the properties of humidity sensors. Nanoparticles, nanowires, and layered nanosheets[8,9] are candidates for the fabrication of high-performance humidity sensors. In particular, metal oxide nanoparticles are excellent moisture-sensitive materials owing to their ability to adsorb oxygen on their surfaces. Zhang et al. reported a three-dimensional mesoporous Co_3O_4 humidity sensor that exhibited good linearity, low hysteresis, a quick response (1 s), and a short recovery time (13.5 s). The excellent sensing performance was attributed to the strong hydrophilicity and unique 3D porous structure of Co_3O_4.[10] In addition, Yu et al. fabricated a porous Co_3O_4 humidity sensor modified by carbon dots (CDs). The CD-Co_3O_4 humidity sensor showed high water vapor selectivity and was capable of sensing slight variations in finger humidity.[11] However, humidity sensors based on metal oxide nanoparticles are restricted by their limited oxygen adsorption capabilities at room temperature. Obtaining better sensing performance at room temperature is still a challenge.

In 1938, F. W. Dunmore fabricated a LiCl humidity sensor. Although LiCl sensed humidity levels effectively, the humidity sensor comprising pure LiCl was easily dissolved at high humidity levels, resulting in a dramatic drop in sensing performance.[12] Metal oxides compounded with hydrophilic inorganic salts provided a pathway to enhancing moisture sensitivity at high humidity levels. Feng et al. reported a LiCl-doped ZnO nanorods/silicon nanoporous pillar capacitive humidity sensor,[13] for which doping remarkedly improved the sensitivity. Zhu et al. reported LiCl-doped SnSe nanosheet humidity sensors. They found that the incorporation of LiCl dramatically decreased the response/recovery time and increased the sensitivity.[14] Qi et al. reported a KCl-doped ZnO nanofiber humidity sensor.[15] Doping with KCl increased the sensitivity and shortened the response time. Subsequently, Song et al. reported KCl-doped SnO_2 nanofibers that exhibited excellent moisture sensing performance.[16]

Recently, the heterostructures of composite materials have attracted interest in the development of humidity sensors. The

Received: November 7, 2022
Accepted: January 17, 2023
Published: January 26, 2023

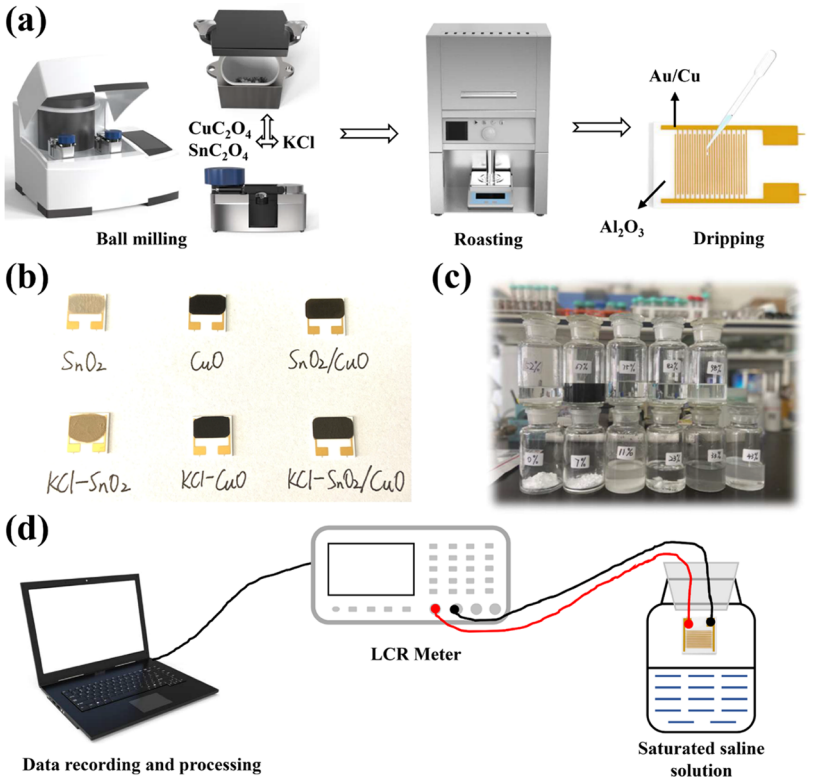

Figure 1. (a) Preparations of moisture-sensitive materials and humidity sensors. (b) Photographs of sensing electrodes. (c) Saturated salt solutions. (d) Humidity testing process.

metal oxide semiconductor heterostructure[17−19] dramatically improved the sensitivity and responsiveness of the sensor owing to the special physicochemical property resulting from energy band bending. Wu et al. reported an rGO-$BiVO_4$ heterostructure humidity sensor that exhibited good repeatability, low hysteresis, and high sensitivity.[20] Given the favorable effects of heterostructures doped with hydrophilic inorganic salts for humidity sensing, it is of interest to incorporate hydrophilic inorganic salts into nanoheterostructures to further improve the sensor performance. However, few reports describing this approach can be found.

As a result, a moisture-sensitive material was prepared in this study by doping KCl into CuO/SnO_2 nanoheterostructures using ball milling−roasting. A humidity sensor was fabricated by depositing the moisture-sensitive material on an interdigital electrode. The nanostructural, morphological, and compositional characteristics of the KCl-doped CuO/SnO_2 were fully examined with X-ray diffraction (XRD), scanning electron microscopy (SEM), transmission electron microscopy (TEM), X-ray photoelectron spectroscopy (XPS), nitrogen sorption analysis, and ultraviolet−visible (UV−vis) spectroscopy. The humidity sensing performance of the sensor based on KCl-doped CuO/SnO_2 was investigated over a wide range of relative humidities (RHs) with a simple homemade device. Compared with previously reported sensors, the sensor based on KCl-doped CuO/SnO_2 exhibited high sensitivity, good linearity, and low hysteresis. The mechanism for sensing water with KCl-doped CuO/SnO_2 was explored. KCl-doped CuO/SnO_2 has great potential for use in health monitoring and environmental detection, given its ultrahigh humidity sensing capability.

2. EXPERIMENTAL SECTION

2.1. Preparation of CuO or SnO_2. One gram of CuC_2O_4 or SnC_2O_4 powder was added to the ball milling tank. The rotation rate, rated power, and ball milling time of the ball milling machine (QM3SP4, Nanjing Shunchi Technology, Co. Ltd., China) were 530 rpm, 1.5 kW, and 10 h, respectively. The rotation direction was changed every 1 h. After ball milling, the powder was dried in a vacuum oven at 60 °C for 12 h. After that, the dried powder was placed in a muffle furnace, heated up to 380 °C at 2 °C min^{-1}, and held at 380 °C for 3 h. Finally, the powder was cooled to room temperature in the furnace. The above reagents were purchased from Shanghai Macklin Biochemical Co., Ltd., China.

2.2. Preparation of KCl-Doped CuO or SnO_2. CuC_2O_4 or SnC_2O_4 and KCl (Shanghai Macklin Biochemical Co., Ltd., China) powders were added to the ball milling tank in a mass ratio of 10:1. The specific ball milling and roasting scheme used was consistent with that described in Section 2.1.

2.3. Preparation of CuO/SnO_2. CuC_2O_4 and SnC_2O_4 powders were added to the ball milling tank in a 1:1 mass ratio. The specific ball milling and roasting scheme used was consistent with that described in Section 2.1.

2.4. Preparation of KCl-Doped CuO/SnO_2. The synthesis of KCl-doped CuO/SnO_2 is shown in Figure 1a. CuC_2O_4 and SnC_2O_4 powders were added to the ball milling tank in a 1:1 mass ratio, and a mass of KCl powder corresponding to one-tenth of the total mass of the above powders was also added. The specific ball milling and roasting scheme used was consistent with that described in Section 2.1.

2.5. Fabrication of Humidity Sensors. The synthesized moisture-sensitive material was dissolved in deionized water to prepare a colloidal solution. The colloidal solution was added

https://doi.org/10.1021/acsomega.2c07098
ACS Omega 2023, 8, 4878−4888

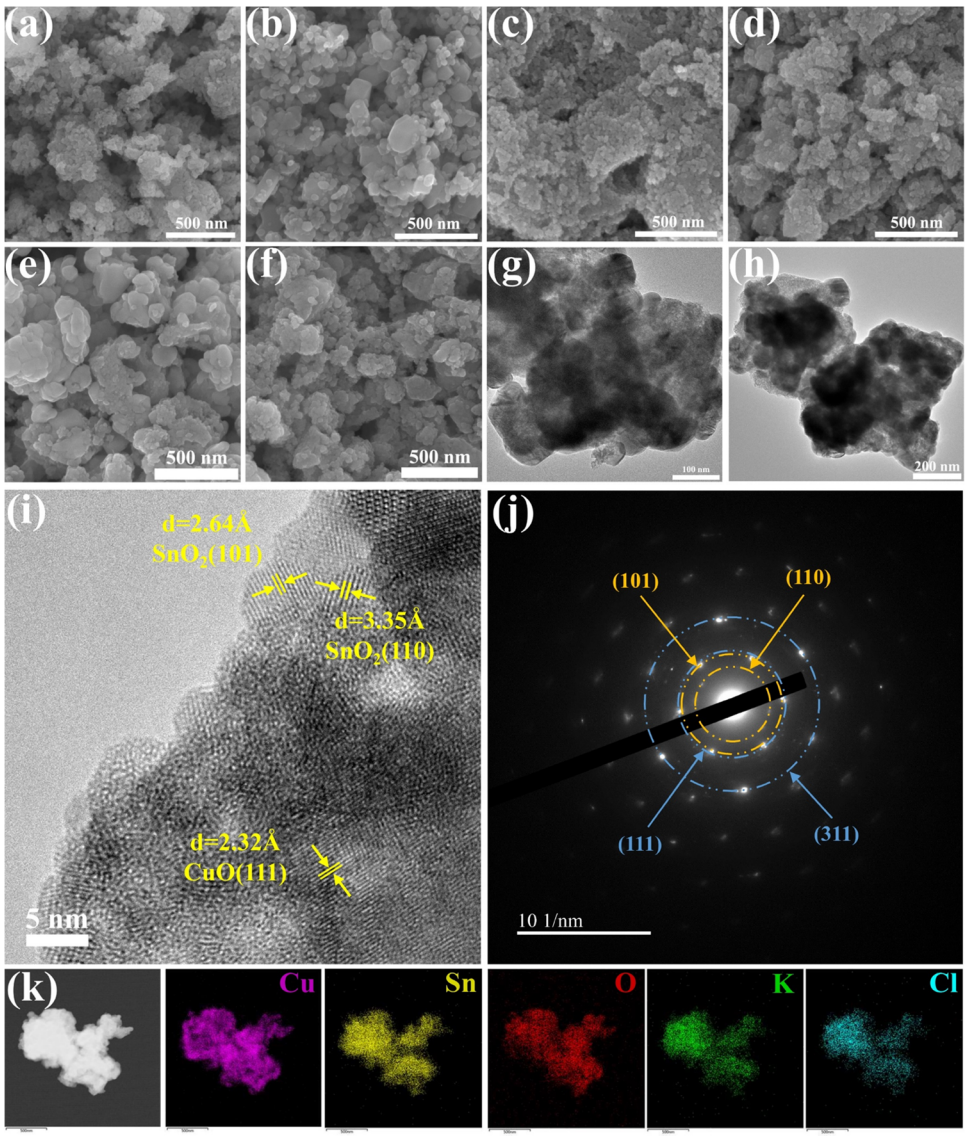

Figure 2. SEM images of (a) CuO, (b) KCl-CuO, (c) SnO_2, (d) KCl-SnO_2, (e) CuO/SnO_2, and (f) KCl-CuO/SnO_2. TEM images of (g) CuO/SnO_2 and (h) KCl-CuO/SnO_2. HRTEM image of (i) KCl-CuO/SnO_2. SAED data for (j) KCl-CuO/SnO_2; the orange and blue marks correspond to SnO_2 and CuO, respectively. EDS maps of (k) KCl-CuO/SnO_2.

dropwise onto the interdigital electrode using a 1 mL pipette gun. The electrode was dried at 80 °C for 6 h to solidify the moisture-sensitive material. Photographs of the fabricated sensing electrodes are shown in Figure 1b.

2.6. Characterization of Moisture-Sensitive Materials. The superficial morphologies and crystal structures of the formulated moisture-sensitive materials were characterized by SEM (Hitachi regulus 8100, Japan) and TEM (Jeoljem-2100, Japan). The crystal structures of the moisture-sensitive materials were characterized by XRD (Rigaku Miniflex 600, Cu Kα, λ = 1.54 Å, Japan). The band gaps were determined via UV−vis spectroscopy (Shimadzu, UV-3600, Japan). The specific surface areas and pore diameters were measured with nitrogen adsorption and desorption (BET, ASAP 2020 PLUS HD88). The elemental compositions and oxidation states of the elements were characterized by XPS (Thermo ESCALAB 250Xi Scanning).

2.7. Humidity Sensing. Humidity sensing was performed with the saturated salt solution method (Figure 1c).[21,22] Solutions of P_2O_5, $CaCl_2$, LiCl, CH_3COOK, $MgCl_2$, K_2CO_3, $Mg(NO_3)_2$, $CuCl_2$, NaCl, KCl, and K_2SO_4 were placed in wide-mouth bottles to provide RH environments of 0, 7, 11, 23, 33, 43, 52, 67, 75, 82, and 97%, respectively. These reagents were purchased from Shanghai Macklin Biochemical Co., Ltd., China. The resistance of the sensor was detected and recorded by a UC 2858B+ (Changzhou Youce Electronic Technology Co., Ltd., China) inductance capacitance resistance (LCR) meter (Figure 1d). The complex impedance spectrum (CIS) was obtained from an electrochemical workstation (Shanghai Chenhua Instrument Co., Ltd., China). The sensor sensitivity was measured as $S = (R_X - R_0)/(RH_X - RH_0)$, where R_X and R_0 are the resistance values of the sensor at the X and 0% RH levels, respectively.[23] When the sensor absorbed and desorbed water molecules, the response/recovery time was defined as that when the resistance of the moisture-sensitive material reached 90% of the total resistance change.

https://doi.org/10.1021/acsomega.2c07098
ACS Omega 2023, 8, 4878−4888

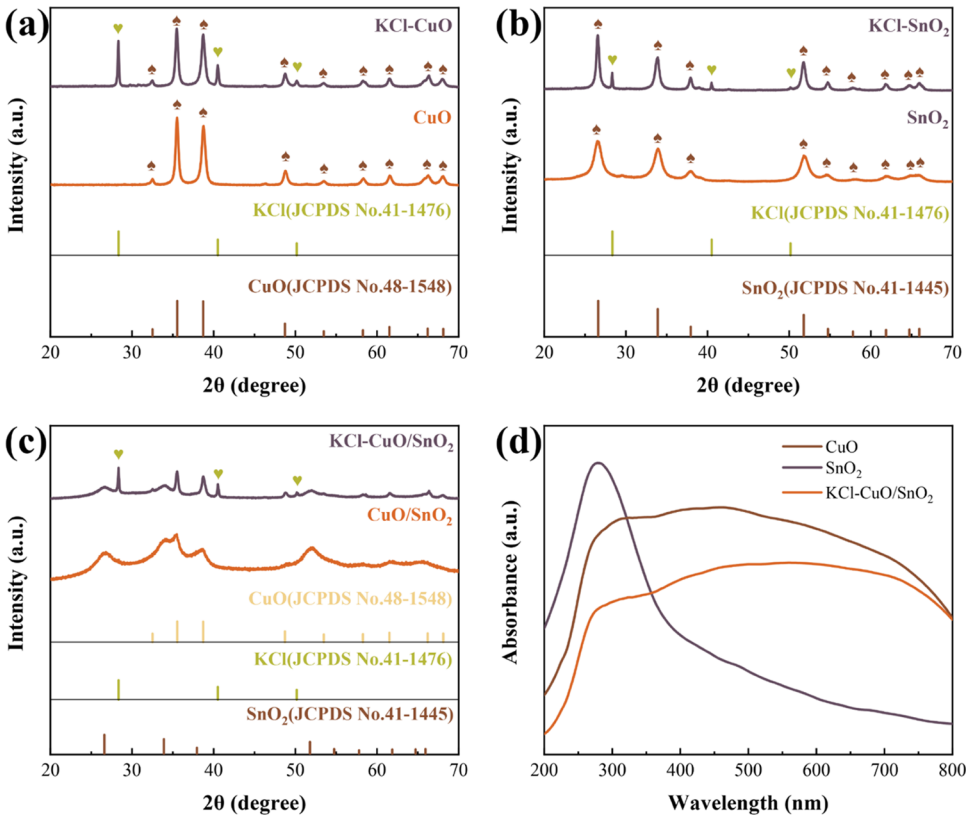

Figure 3. (a) XRD patterns for CuO and KCl-CuO. (b) XRD patterns for SnO_2 and KCl-SnO_2. (c) XRD patterns for CuO/SnO_2 and KCl-CuO/SnO_2. (d) UV−vis spectra of CuO, SnO_2, and KCl-CuO/SnO_2.

3. RESULTS AND DISCUSSION

3.1. Material Characterizations. Figure 2a−f presents the surface morphologies of CuO, KCl-CuO, SnO_2, KCl-SnO_2, CuO/SnO_2, and KCl-CuO/SnO_2, respectively. The particle sizes of the KCl-CuO/SnO_2 composites were smaller than 100 nm (Figure 2g,h). The surface morphology of KCl-CuO/SnO_2 was investigated by high-resolution TEM (HRTEM). As shown in Figure 2i, the interplanar spacings (d) were 2.32, 2.64, and 3.35 Å, which were consistent with reported values for the (111) plane of CuO and the (101) and (110) planes of SnO_2, respectively, indicating the formation of CuO/SnO_2 heterostructures.[24] The presence of periclases CuO and SnO_2 was also confirmed by the selected area electron diffraction (SAED) pattern (Figure 2j), which showed diffraction rings corresponding to reflections of CuO and SnO_2. The elemental compositions and distributions of the KCl-CuO/SnO_2 composites were evaluated by energy-dispersive X-ray spectroscopy (EDS) mapping. The uniform distributions of Cu, Sn, O, K, and Cl are shown in Figure 2k, indicating the formulation of the KCl-CuO/SnO_2 composite.

The XRD patterns for the synthesized CuO, KCl-CuO, SnO_2, and KCl-SnO_2 nanoparticles (Figure 3a,b) showed diffraction peaks in the range 10−70°. The reflection peaks for CuO/SnO_2 and KCl-CuO/SnO_2 (Figure 3c) corresponded exactly to the diffraction peaks for KCl, CuO, and SnO_2. The band gap was calculated from the UV−vis spectrum.[20] As shown in Figure 3d, CuO, SnO_2, and KCl-CuO/SnO_2 primarily absorbed UV light at a wavelength of 280 nm. The band gaps of CuO, SnO_2, and KCl-CuO/SnO_2 were 1.7, 3.3, and 1.5 eV, respectively (Figures S1−S33). Compared with CuO and SnO_2, KCl-CuO/SnO_2 has a lower band gap. The formed heterostructures provided special physicochemical properties. The unimpeded and rapid migration of carriers enhanced the sensitivity and response speed for humidity sensing.[25]

The materials CuO, KCl-CuO, SnO_2, KCl-SnO_2, CuO/SnO_2, and KCl-CuO/SnO_2 exhibited Type-IV isotherms for nitrogen adsorption/desorption (Figure 4a−c). The incorporation of KCl reduced the specific surface area, which likely resulted from the agglomeration of nanoparticles due to the infiltration of KCl. The KCl-CuO/SnO_2 had a larger specific surface area than KCl-CuO and KCl-SnO_2. As shown in Figures S4−S6, more macropores (diameter higher than 50 nm) appeared upon incorporation of KCl into CuO, SnO_2, and CuO/SnO_2, suggesting that the dispersion of KCl in the materials altered the topological morphologies of the pores.

Figure 4d illustrates the full XPS spectrum of KCl-CuO/SnO_2 and confirms the existence of Cu, Sn, O, K, and Cl elements. The peaks at 934.6 and 954.5 eV in the Cu 2p spectrum (Figure 4e) corresponded to Cu $2p_{3/2}$ and Cu $2p_{1/2}$ binding energies, with satellite peaks at 942.1, 944.5, and 963.0 eV (labeled as Sat).[26] The peaks at 494.8 and 486.3 eV (Figure 4f) corresponded to Sn $3d_{3/2}$ and Sn $3d_{5/2}$ binding energies, respectively. The peak at 529.7 eV (Figure 4g) was assigned to the oxygens of the CuO and SnO_2 lattices, while the peak at 531.0 eV was ascribed to surface adsorbed oxygen.[27] The peaks at 295.9 and 293.0 eV (Figure 4h) corresponded to K $2p_{1/2}$ and K $2p_{3/2}$ binding energies, respectively.[28] The peak at 198.8 eV (Figure 4i) was assigned to ionization of the Cl $2p_{3/2}$ state.[29] Therefore, the formation of the CuO/$Ti_3C_2T_X$ heterostructure was further verified.

https://doi.org/10.1021/acsomega.2c07098
ACS Omega 2023, 8, 4878−4888

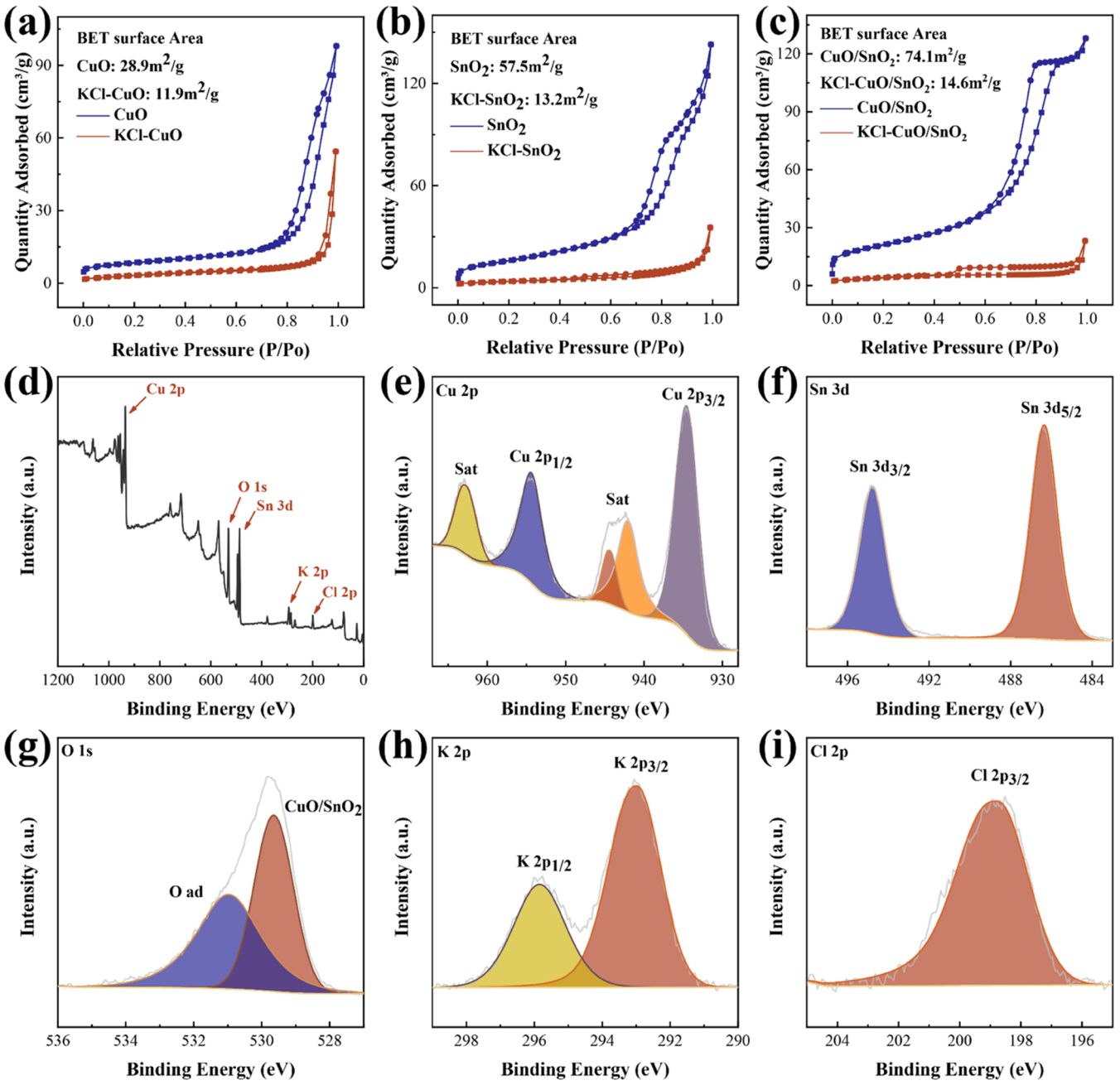

Figure 4. Nitrogen adsorption and desorption isotherms of (a) CuO and KCl-CuO, (b) SnO_2 and KCl-SnO_2, and (c) CuO/SnO_2 and KCl-CuO/SnO_2. XPS spectra of KCl-CuO/SnO_2 composites, including (d) the full scan spectrum and (e) Cu 2p, (f) Sn 3d, (g) O 1s, (h) K 2p, and (i) Cl 2p spectra.

Table 1. Moisture-Sensitive Properties of the Six Samples

samples	CuO	KCl-CuO	SnO_2	KCl-SnO_2	CuO/SnO_2	KCl-CuO/SnO_2
sensitivity (kΩ/%RH)	0.12	2.36	0.004	0.31	141	194
detection range (RH)	0−97%	0−97%	0−97%	0−97%	0−97%	0−97%
response/recovery time (s)	6.0/8.5	4.0/5.0	3.0/5.0	2.0/2.5	6.0/9.0	1.0/1.5

3.2. Humidity Sensing Performances. The humidity sensing data were determined at 26 °C. Table 1 shows the humidity sensing data obtained for the six samples at 100 Hz. The sensitivities of the pure CuO and pure SnO_2 sensors were poor. The KCl-doped samples showed higher sensitivities and faster response/recovery times than the undoped ones. The CuO/SnO_2 and KCl-CuO/SnO_2 sensors exhibited high sensitivity, which was attributed to the special physicochemical properties of the semiconductor heterostructures. Therefore, both KCl doping and the CuO/SnO_2 p−n heterostructures led to high sensitivities and fast response/recovery times.

Figure 5a compares the resistance values of the six sensors, which were determined at 100 Hz and with different RH values. Except for the CuO sensor, the resistance values of all

https://doi.org/10.1021/acsomega.2c07098
ACS Omega 2023, 8, 4878−4888

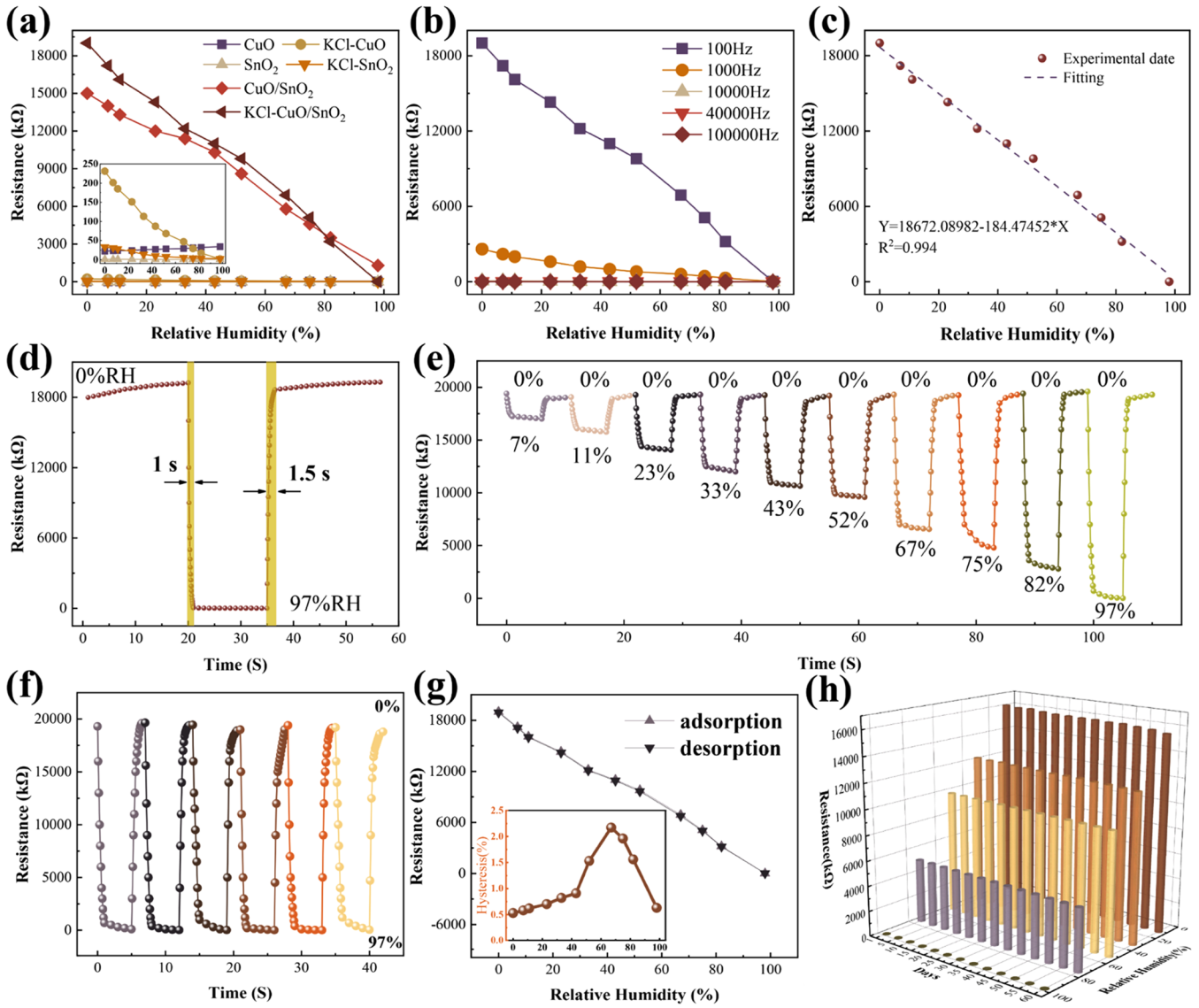

Figure 5. (a) Plots of resistance as a function of RH at 100 Hz for the six sensors. The inset shows a partially enlarged drawing. (b) Plots of resistance as a function of RH at different frequencies for the KCl-CuO/SnO_2 sensor. (c) Fit for a plot of resistance versus RH for the KCl-CuO/SnO_2 sensor at 100 Hz. (d) Resistance as a function of time at 100 Hz for the KCl-CuO/SnO_2 sensor. The humidity sensing performance of KCl-CuO/SnO_2 sensors; (e) dynamic response of the sensor; (f) repeatability; and (g) resistance as a function of RH during adsorption and desorption. The inset shows humidity hysteresis with various RHs; (h) plots indicating stability.

Table 2. Comparison of the Sensor Prepared in this Work with Previously Reported Humidity Sensors

material	sensing mechanism	detection range (RH) (%)	sensitivity (kΩ/%RH)	response/recovery time (s)	reference
Ti_3C_2/polyelectrolyte	resistive	10−70	1.6	0.11/0.22	30
MoS_2/PEO	resistive	0−80	85	0.6/0.3	31
hBN/PEO	impedance	0−90	24	2.6/2.8	32
PAM, Cr_3C_2	impedance	0−90	0.66	1.0/1.9	33
PEDOT: PSS/MoS_2 flakes	impedance	0−80	50	0.5/0.8	34
KCl-CuO/SnO_2	resistive	0−97	194	1.0/1.5	this work

sensors declined with increases in RH. Figure 5b shows plots of the resistance as a function of RH at different frequencies for the KCl-CuO/SnO_2 sensor. The highest sensitivity of 194 kΩ/%RH was achieved at 100 Hz. Consequently, 100 Hz was used in the subsequent experiments to obtain the optimal sensing performance. Figure 5c illustrates the fit for a plot of resistance data versus RH for the KCl-CuO/SnO_2 sensor at 100 Hz. Excellent linearity resulted for KCl-CuO/SnO_2 with a regression coefficient R^2 of 0.994. As shown in Figure 5d, the response time and recovery time of KCl-CuO/SnO_2 were 1 and 1.5 s, respectively.

Figure 5e demonstrates the dynamic response of the KCl-CuO/SnO_2 sensor at different RH values. As shown in Figure 5f, the resistance values for the KCl-CuO/SnO_2 sensor were nearly identical for each RH cycle over the range 0−97%, indicating excellent repeatability. The hysteresis behavior of

https://doi.org/10.1021/acsomega.2c07098
ACS Omega 2023, 8, 4878−4888

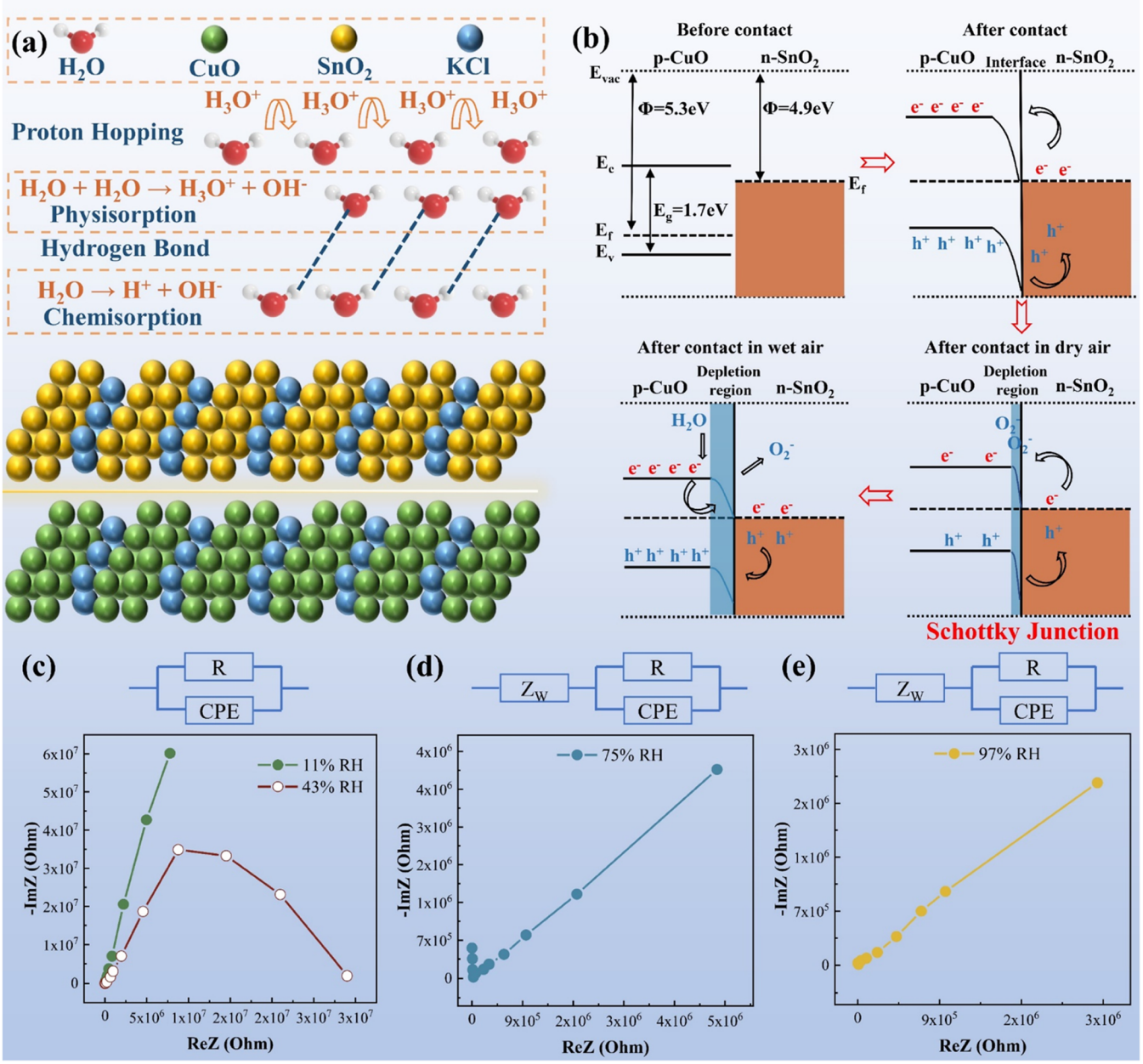

Figure 6. (a) Schematic diagram for water molecule adsorption. (b) Energy band diagram of the KCl-CuO/SnO_2 heterostructure. (c–e) Complex impedance plots of KCl-CuO/SnO_2 at 11, 43, 75, and 97% RH. Inset: the EC corresponding to the complex impedance spectrum.

the KCl-CuO/SnO_2 sensor during adsorption (RH was increased from 0 to 97%) and desorption (RH was decreased from 97 to 0%) is shown in Figure 5g. The equation for the humidity hysteresis value at different RH values is $H = (R_{ads} - R_{des})/S \times 100\%$, where R_{ads} and R_{des} are the resistance values during adsorption and desorption, respectively.[35] As shown in the inset of Figure 5g, the hysteresis values were below 2.5%. Notably, the hysteresis values gradually converged to 0.5 below an RH level of 43%, indicating that the sensor was highly reversible at low RH. The KCl-CuO/SnO_2 sensor exhibited stable resistance for over 60 days (Figure 5h), indicating good long-term stability.

Table 2 compares the humidity sensing behaviors of previously reported sensors and our fabricated KCl-CuO/SnO_2 sensor. The resistance humidity sensor detects changes in the resistance caused by exposure of the material to different humidities. In contrast, the impedance humidity sensor measures variations in the impedance values of the material. Naturally, resistive sensors exhibit the characteristics of simple structures, convenient testing, and wide application ranges. Compared with the resistive and impedance sensors, the KCl-CuO/SnO_2 sensor exhibited a higher sensitivity and a wider detection range. It should be noted that the KCl-CuO/SnO_2 sensor was not satisfactory in terms of response/recovery time compared to the two resistive sensors that were fabricated from a two-dimensional (2D) material,[30−32,34] as shown in Table 2. This short response/recovery time of 2D material-based sensors was attributed to the inherently hydrophilic functional groups, large specific surface area, and superior electrical conductivity of the 2D material.

3.3. Humidity Sensing Mechanism. Figure 6a shows that at low RH, chemisorption of water molecules occurred on the

https://doi.org/10.1021/acsomega.2c07098
ACS Omega 2023, 8, 4878−4888

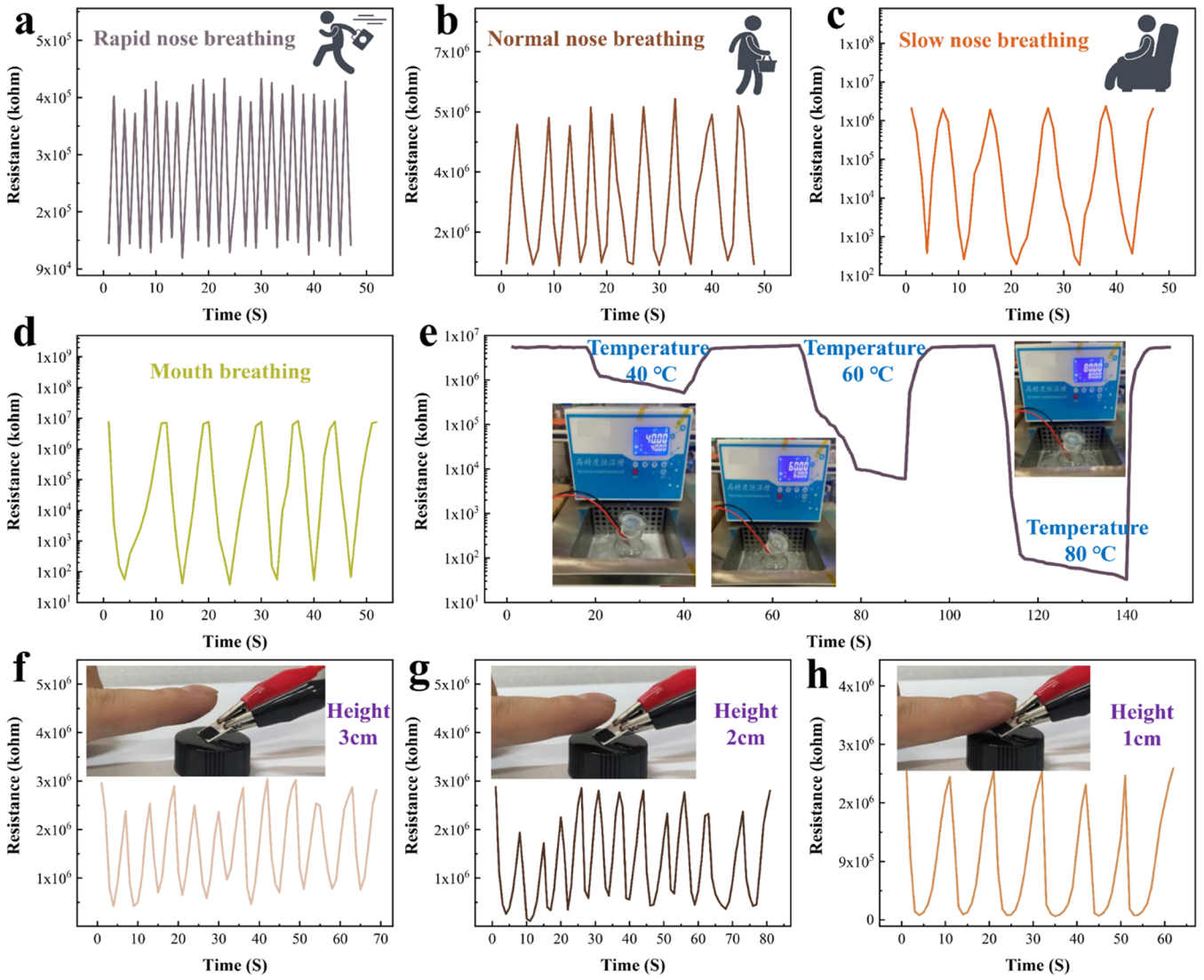

Figure 7. Applications of the KCl-CuO/SnO_2 sensor in daily life. (a) Rapid nose breathing. (b) Normal nose breathing. (c) Slow nose breathing. (d) Mouth breathing. (e) Water vapor testing at different temperatures. Noncontact finger humidity detection at (f) a height of 3 cm; (g) a height of 2 cm; and (h) a height of 1 cm.

KCl-CuO/SnO_2 surface. Moreover, hydrogen bonds were formed between the water molecules. Given the presence of water molecules, KCl dissociated into K^+ and Cl^- and enhanced the conductivity, resulting in high sensor sensitivity even under low RH conditions.[29] With a further increase in RH, the water molecules underwent physical adsorption and were protonated to H_3O^+. Furthermore, proton hopping on the KCl-CuO/SnO_2 surface occurred, which can be explained by Grotthuss' ion-transfer mechanism.[36,37] Due to the porous structure of the KCl-CuO/SnO_2 and the hydrophilicity of KCl, many water molecules were incorporated into the pores and generated high sensitivity.

Compared with the favorable effects of hydrophilic KCl, the CuO/SnO_2 heterostructure improved the sensitivity and response speed of the sensor to a greater extent. To illustrate the mechanism for enhanced humidity sensing by the CuO/SnO_2 heterostructures, energy band diagrams are provided in Figure 6b. CuO is a typical p-type semiconductor for which the humidity sensing mechanism can be explained by the adsorption and desorption of oxygen molecules.[38] Oxygen molecules adsorbed on the CuO surface in a dry room environment trap electrons such that the hole concentration of the CuO increases and the resistance decreases. Conversely, oxygen ions adsorbed on the CuO surface in a moist environment are replaced by water molecules, leading to an increase in resistance because the trapped electrons are released back into the CuO. On the other hand, SnO_2 is an n-type semiconductor with a humidity sensing mechanism different from that of CuO.[39] In a dry environment, adsorbed oxygen molecules on the surface of SnO_2 accept electrons and decrease the electron concentration, increasing the sensor resistance. When the RH increases, the oxygen ions adsorbed on the SnO_2 surface are substituted by water molecules, and the trapped electrons are released back to the SnO_2, resulting in a decrease in the resistance of the sensor.

CuO (5.3 eV)[40,41] and SnO_2 (4.9 eV)[42] exhibit different work functions. Therefore, electrons are transferred from SnO_2 to CuO to effect Fermi-level equality and form a p−n heterojunction due to the interaction of CuO and SnO_2. Furthermore, Schottky barriers and electron depletion regions are formed at the interfaces between CuO and SnO_2.

https://doi.org/10.1021/acsomega.2c07098
ACS Omega 2023, 8, 4878−4888

In a dry environment, the CuO/SnO_2 sensor adsorbs oxygen at the interfaces between CuO and SnO_2 and captures electrons. Given the reduction of the electrons, the electron depletion region becomes thinner, and the energy band bends upward, which leads to increased resistivity. In the case of wet air, the oxygen ions at the CuO/SnO_2 interface are supplanted by water molecules, and the originally trapped electrons are released. The increase in the number of electrons results in a thickened electron depletion region, a downward-bending energy band, and a decreased resistance. Briefly, the formation of a p−n heterojunction obviously increases the resistance of the composite in dry air and decreases the resistance of the composite in high-humidity air, leading to a remarkable enhancement in the sensing response. In addition, the presence of p−n heterojunctions contributes to an increase in the interfacial hole−electron separation rate, which enables the electrons to be more easily trapped by chemisorbed oxygen. Consequently, the recovery time is reduced to some extent.

We further investigated the moisture sensing mechanism of KCl-CuO/SnO_2 with CIS diagrams. Figure 6c−e displays the impedance values of KCl-CuO/SnO_2 at various working frequencies (from 50 Hz to 1 MHz). The CIS curves exhibited incomplete semicircles in lower humidity environments (11% RH). This may be attributed to the inherent conductivity of the KCl-CuO/SnO_2 composites, reflecting weak ionic conductivity at low RH.[43] At low relative humidity, the CIS can be characterized with an equivalent circuit (EC) comprising a shunt resistor (R) and a capacitor (CPE). With increases in the RH (from 43 to 97% RH), the CIS curve exhibited a semicircular tail in the low-frequency region. The shape became more pronounced with increases in the RH. This was ascribed to H_3O^+ diffusion through the KCl-CuO/SnO_2 nanocomposite structure, which was explained by the Warburg impedance.[44,45] CIS at high humidity can be depicted as EC with parallel capacitance and resistance and series Warburg impedance (Z_W). Consequently, the humidity sensors based on KCl-CuO/SnO_2 composites demonstrated outstanding sensitivity to humidity, especially at low RH levels.

3.4. Application. Humidity measurements with the KCl-CuO/SnO_2 sensor in ordinary life were investigated to confirm the ultrahigh sensitivity and rapid response. Figure 7a−c shows application of KCl-CuO/SnO_2 sensors in monitoring nose respiration. The KCl-CuO/SnO_2 sensor distinguished between different rates of nasal respiration and exhibited different responses. In addition, the sensor was used to test mouth breathing and demonstrated extremely good reproducibility (Figure 7d).

Figure 7e shows that the KCl-CuO/SnO_2 sensor was applicable for determinations of water vapor at different temperatures. Accordingly, the temperature of the water could be inferred from the response of the sensor. The KCl-CuO/SnO_2 sensor also showed an excellent response for noncontact sensing of finger humidity. Figure 7f−h illustrates the responses of the sensor when the human finger was placed 3 cm, 2 cm, and 1 cm away from the sensor, respectively. Thus, the KCl-CuO/SnO_2 sensor has enormous potential for application in contactless sensing and other fields. In future studies, the resistance of the sensor based on KCl-doped CuO/SnO_2 p−n heterostructures must be decreased further to reduce power consumption. In addition, the response/recovery time of the sensor must be further shortened for better performance in monitoring, for example, respiration and contactless human-computer interactions.

4. CONCLUSIONS

In summary, we have successfully fabricated KCl-CuO/SnO_2 composites by ball milling−roasting methods and employed them for humidity detection. The successful synthesis of the KCl-CuO/SnO_2 composite was demonstrated by SEM, TEM, XRD, and XPS. Nitrogen adsorption and desorption experiments showed that doping with KCl decreased the specific surface areas of CuO/SnO_2 composites, indicating that KCl was successfully adsorbed in the porous structure of CuO/SnO_2. The KCl-doped CuO/SnO_2 humidity sensor showed a superb linear response, low hysteresis, strong stability, a high sensitivity of 194 kΩ/%RH, and a short response time of 1 s. The water adsorption principles and energy band structure of the KCl-CuO/SnO_2 composites indicated that the excellent humidity sensing performance originated from the ionic conductivity of KCl, the formation of heterojunctions, a change in the Schottky barrier height, and depletion of electronic depletion layers. These results showed that KCl-CuO/SnO_2 composites are promising humidity sensing materials that can be used in respiratory monitoring, contactless sensing, and environmental monitoring.

■ ASSOCIATED CONTENT

Supporting Information

The Supporting Information is available free of charge at https://pubs.acs.org/doi/10.1021/acsomega.2c07098.

Detailed UV−vis spectra; detailed material pore size (PDF)

■ AUTHOR INFORMATION

Corresponding Author

Xinhai Yu − *MOE Key Laboratory of Pressure Systems and Safety, East China University of Science and Technology, Shanghai 200237, P. R. China; School of Mechanical and Power Engineering, East China University of Science and Technology, Shanghai 200237, P. R. China;* orcid.org/0000-0001-6391-5062; Email: yxhh@ecust.edu.cn

Authors

Lei Wang − *MOE Key Laboratory of Pressure Systems and Safety, East China University of Science and Technology, Shanghai 200237, P. R. China; School of Mechanical and Power Engineering, East China University of Science and Technology, Shanghai 200237, P. R. China;* orcid.org/0000-0002-2113-4644

Feng Huang − *MOE Key Laboratory of Pressure Systems and Safety, East China University of Science and Technology, Shanghai 200237, P. R. China; School of Mechanical and Power Engineering, East China University of Science and Technology, Shanghai 200237, P. R. China*

Xinqi Yao − *MOE Key Laboratory of Pressure Systems and Safety, East China University of Science and Technology, Shanghai 200237, P. R. China; School of Mechanical and Power Engineering, East China University of Science and Technology, Shanghai 200237, P. R. China*

Shuaishuai Yuan − *MOE Key Laboratory of Pressure Systems and Safety, East China University of Science and Technology, Shanghai 200237, P. R. China; School of Mechanical and Power Engineering, East China University of Science and Technology, Shanghai 200237, P. R. China*

Shan-Tung Tu − *MOE Key Laboratory of Pressure Systems and Safety, East China University of Science and Technology,*

https://doi.org/10.1021/acsomega.2c07098
ACS Omega 2023, 8, 4878−4888

Shanghai 200237, P. R. China; School of Mechanical and Power Engineering, East China University of Science and Technology, Shanghai 200237, P. R. China

Shijian Chen − *SUFA Technology Industry Co., Ltd., CNNC, Suzhou 215001, P. R. China*

Complete contact information is available at: https://pubs.acs.org/10.1021/acsomega.2c07098

Author Contributions

The manuscript was written through contributions of all authors. All authors have given approval to the final version of the manuscript.

Notes

The authors declare no competing financial interest.

■ ACKNOWLEDGMENTS

This work was financially supported by the National Key Research and Development Program of China [2018YFA0704604].

■ REFERENCES

(1) Fan, Y.; Liu, W.; Li, S.; Chowwanonthapunya, T.; Wongpat, B.; Zhao, Y.; Dong, B.; Zhang, T.; Li, X. Evolution of Rust Layers on Carbon Steel and Weathering Steel in High Humidity and Heat Marine Atmospheric Corrosion. *J. Mater. Sci. Technol.* **2020**, *39*, 190−199.

(2) Sotoodeh, K. A Review of Valve Stem Sealing to Prevent Leakage from the Valve and Its Effect on Valve Operation. *J Fail. Anal. and Preven.* **2021**, *21*, 9−16.

(3) Kim, S. H.; Rhee, M. S. Environment-Friendly Mild Heat and Relative Humidity Treatment Protects Sprout Seeds (Radish, Mung Bean, Mustard, and Alfalfa) against Various Foodborne Pathogens. *Food Control* **2018**, *93*, 17−22.

(4) Allison, L. K.; Rostaminia, S.; Kiaghadi, A.; Ganesan, D.; Andrew, T. L. Enabling Longitudinal Respiration Monitoring Using Vapor-Coated Conducting Textiles. *ACS Omega* **2021**, *6*, 31869−31875.

(5) Yi, Y.; Jiang, Y.; Zhao, H.; Brambilla, G.; Fan, Y.; Wang, P. High-Performance Ultrafast Humidity Sensor Based on Microknot Resonator-Assisted Mach−Zehnder for Monitoring Human Breath. *ACS Sens.* **2020**, *5*, 3404−3410.

(6) Xu, L.; Zhai, H.; Chen, X.; Liu, Y.; Wang, M.; Liu, Z.; Umar, M.; Ji, C.; Chen, Z.; Jin, L.; Liu, Z.; Song, Q.; Yue, P.; Li, Y.; Ye, T. T. Coolmax/Graphene-Oxide Functionalized Textile Humidity Sensor with Ultrafast Response for Human Activities Monitoring. *Chem. Eng. J.* **2021**, *412*, No. 128639.

(7) Delipinar, T.; Shafique, A.; Gohar, M. S.; Yapici, M. K. Fabrication and Materials Integration of Flexible Humidity Sensors for Emerging Applications. *ACS Omega* **2021**, *6*, 8744−8753.

(8) Ryu, B.; Wang, L.; Pu, H.; Chan, M. K. Y.; Chen, J. Understanding, Discovery, and Synthesis of 2D Materials Enabled by Machine Learning. *Chem. Soc. Rev.* **2022**, *51*, 1899−1925.

(9) Bian, R.; Li, C.; Liu, Q.; Cao, G.; Fu, Q.; Meng, P.; Zhou, J.; Liu, F.; Liu, Z. Recent Progress in the Synthesis of Novel Two-Dimensional van Der Waals Materials. *Natl. Sci. Rev.* **2022**, *9*, No. nwab164.

(10) Zhang, Y.; Wu, Y.; Duan, Z.; Liu, B.; Zhao, Q.; Yuan, Z.; Li, S.; Liang, J.; Jiang, Y.; Tai, H. High Performance Humidity Sensor Based on 3D Mesoporous Co_3O_4 Hollow Polyhedron for Multifunctional Applications. *Appl. Surf. Sci.* **2022**, *585*, No. 152698.

(11) Yu, H.; Wang, C.; Meng, F.; Xiao, J.; Liang, J.; Kim, H.; Bae, S.; Zou, D.; Kim, E.-S.; Kim, N.-Y.; Zhao, M.; Li, B. Microwave Humidity Sensor Based on Carbon Dots-Decorated MOF-Derived Porous Co3O4 for Breath Monitoring and Finger Moisture Detection. *Carbon* **2021**, *183*, 578−589.

(12) Li, N.; Li, X.; Zhang, T.; Qiu, S.; Zhu, G.; Zheng, W.; Yu, W. Host−Guest Composite Materials of LiCl/NaY with Wide Range of Humidity Sensitivity. *Mater. Lett.* **2004**, *58*, 1535−1539.

(13) Feng, M. H.; Li, X. J. Capacitive Humidity-Sensing Properties of ZnO Nanorods/Silicon Nanoporous Pillar Array Enhanced by LiCl Incorporation. *Sens. Actuators, B* **2018**, *272*, 543−549.

(14) Zhu, K.; Tang, Y.; Zhong, X.; Xiong, L.; Zhang, Y.; Tan, C.; Song, H.; Wang, J. Improved Response/Recovery Time and Sensitivity of SnSe Nanosheet Humidity Sensor by LiCl Incorporation. *Adv. Electron. Mater.* **2020**, *6*, No. 1901330.

(15) Qi, Q.; Zhang, T.; Wang, S.; Zheng, X. Humidity Sensing Properties of KCl-Doped ZnO Nanofibers with Super-Rapid Response and Recovery. *Sens. Actuators, B* **2009**, *137*, 649−655.

(16) Song, X.; Qi, Q.; Zhang, T.; Wang, C. A Humidity Sensor Based on KCl-Doped SnO_2 Nanofibers. *Sens. Actuators, B* **2009**, *138*, 368−373.

(17) Chen, G.; Wang, H.; Wei, X.; Wu, Y.; Gu, W.; Hu, L.; Xu, D.; Zhu, C. Efficient Z-Scheme Heterostructure Based on TiO_2/$Ti_3C_2T_X$/Cu_2O to Boost Photoelectrochemical Response for Ultrasensitive Biosensing. *Sens. Actuators, B* **2020**, *312*, No. 127951.

(18) Li, R.; Ma, X.; Li, J.; Cao, J.; Gao, H.; Li, T.; Zhang, X.; Wang, L.; Zhang, Q.; Wang, G.; Hou, C.; Li, Y.; Palacios, T.; Lin, Y.; Wang, H.; Ling, X. Flexible and High-Performance Electrochromic Devices Enabled by Self-Assembled 2D TiO_2/MXene Heterostructures. *Nat. Commun.* **2021**, *12*, No. 1587.

(19) Zhang, Z.; Huang, Z.; Li, J.; Wang, D.; Lin, Y.; Yang, X.; Liu, H.; Liu, S.; Wang, Y.; Li, B.; Duan, X.; Duan, X. Endoepitaxial Growth of Monolayer Mosaic Heterostructures. *Nat. Nanotechnol.* **2022**, *17*, 493−499.

(20) Wu, Z.; Sun, X.; Guo, X.; Ding, Y.; Ou, Y.; Yang, H.; Chen, Y.; Hu, Y.; Kuang, D.; Zhao, C.; He, Y. Development of a RGO-$BiVO_4$ Heterojunction Humidity Sensor with Boosted Performance. *ACS Appl. Mater. Interfaces* **2021**, *13*, 27188−27199.

(21) Zhang, D.; Tong, J.; Xia, B.; Xue, Q. Ultrahigh Performance Humidity Sensor Based on Layer-by-Layer Self-Assembly of Graphene Oxide/Polyelectrolyte Nanocomposite Film. *Sens. Actuators, B* **2014**, *203*, 263−270.

(22) Kuang, Q.; Lao, C.; Wang, Z. L.; Xie, Z.; Zheng, L. High-Sensitivity Humidity Sensor Based on a Single SnO_2 Nanowire. *J. Am. Chem. Soc.* **2007**, *129*, 6070−6071.

(23) Liu, X.; Zhang, D.; Wang, D.; Li, T.; Song, X.; Kang, Z. A Humidity Sensing and Respiratory Monitoring System Constructed from Quartz Crystal Microbalance Sensors Based on a Chitosan/Polypyrrole Composite Film. *J. Mater. Chem. A* **2021**, *9*, 14524−14533.

(24) Pandey, M.; Singh, M.; Wasnik, K.; Gupta, S.; Patra, S.; Gupta, P. S.; Pareek, D.; Chaitanya, N. S. N.; Maity, S.; Reddy, A. B. M.; Tilak, R.; Paik, P. Targeted and Enhanced Antimicrobial Inhibition of Mesoporous ZnO−Ag_2O/Ag, ZnO−CuO, and ZnO−SnO_2 Composite Nanoparticles. *ACS Omega* **2021**, *6*, 31615−31631.

(25) Gasso, S.; Sohal, M. K.; Mahajan, A. MXene Modulated SnO_2 Gas Sensor for Ultra-Responsive Room-Temperature Detection of NO_2. *Sensor. Actuators, B* **2022**, *357*, No. 131427.

(26) Li, K.; Lei, Y.; Liao, J.; Zhang, Y. Facile Synthesis of MXene-Supported Copper Oxide Nanocomposites for Catalyzing the Decomposition of Ammonium Perchlorate. *Inorg. Chem. Front.* **2021**, *8*, 1747−1761.

(27) Zhu, L. Y.; Yuan, K.; Yang, J. G.; Ma, H. P.; Wang, T.; Ji, X. M.; Feng, J. J.; Devi, A.; Lu, H. L. Fabrication of Heterostructured p-CuO/n-SnO_2 Core-Shell Nanowires for Enhanced Sensitive and Selective Formaldehyde Detection. *Sens. Actuators, B* **2019**, *290*, 233−241.

(28) Zhang, Q.; Chen, P.; Chen, L.; Wu, M.; Dai, X.; Xing, P.; Lin, H.; Zhao, L.; He, Y. Facile Fabrication of Novel Ag_2S/K-g-C_3N_4 Composite and Its Enhanced Performance in Photocatalytic H_2 Evolution. *J. Colloid Interface Sci.* **2020**, *568*, 117−129.

(29) Guo, C.-y.; Hu, Q.; Xu, Y.; Zhang, X.; Gao, S.; Zhao, H.; Xu, M.; Cheng, X.; Huo, L. KCl-Modified Dy_2O_3 Nanospheres with

Humidity Response for Human Respiration Monitoring. *ACS Appl. Nano Mater.* **2021**, *4*, 9113−9122.
(30) An, H.; Habib, T.; Shah, S.; Gao, H.; Patel, A.; Echols, I.; Zhao, X.; Radovic, M.; Green, M. J.; Lutkenhaus, J. L. Water Sorption in MXene/Polyelectrolyte Multilayers for Ultrafast Humidity Sensing. *ACS Appl. Nano Mater.* **2019**, *2*, 948−955.
(31) Zeeshan Yousaf, H. M.; Kim, S. W.; Hassan, G.; Karimov, K.; Choi, K. H.; Sajid, M. Highly Sensitive Wide Range Linear Integrated Temperature Compensated Humidity Sensors Fabricated Using Electrohydrodynamic Printing and Electrospray Deposition. *Sensor. Actuators, B* **2020**, *308*, No. 127680.
(32) Sajid, M.; Kim, H. B.; Lim, J. H.; Choi, K. H. Liquid-Assisted Exfoliation of 2D hBN Flakes and Their Dispersion in PEO to Fabricate Highly Specific and Stable Linear Humidity Sensors. *J. Mater. Chem. C* **2018**, *6*, 1421−1432.
(33) Kim, H. B.; Sajid, M.; Kim, K. T.; Na, K. H.; Choi, K. H. Linear Humidity Sensor Fabrication Using Bi-Layered Active Region of Transition Metal Carbide and Polymer Thin Films. *Sens. Actuators, B* **2017**, *252*, 725−734.
(34) Siddiqui, G. U.; Sajid, M.; Ali, J.; Kim, S. W.; Doh, Y. H.; Choi, K. H. Wide Range Highly Sensitive Relative Humidity Sensor Based on Series Combination of MoS_2 and PEDOT:PSS Sensors Array. *Sens. Actuators, B* **2018**, *266*, 354−363.
(35) Si, R.; Xie, X.; Li, T.; Zheng, J.; Cheng, C.; Huang, S.; Wang, C. TiO_2/(K,Na)NbO_3 Nanocomposite for Boosting Humidity-Sensing Performances. *ACS Sens.* **2020**, *5*, 1345−1353.
(36) Ernsberger, F. M. The Nonconformist Ion. *J. Am. Ceram. Soc.* **1983**, *66*, 747−750.
(37) Agmon, N. The Grotthuss Mechanism. *Chem. Phys. Lett.* **1995**, *244*, 456−462.
(38) Nitta, R.; Lin, H.-E.; Kubota, Y.; Kishi, T.; Yano, T.; Matsushita, N. CuO Nanostructure-Based Flexible Humidity Sensors Fabricated on PET Substrates by Spin-Spray Method. *Appl. Surf. Sci.* **2022**, *572*, No. 151352.
(39) He, T.; Liu, W.; Lv, T.; Ma, M.; Liu, Z.; Vasiliev, A.; Li, X. MXene/SnO_2 Heterojunction Based Chemical Gas Sensors. *Sens. Actuators, B* **2021**, *329*, No. 129275.
(40) Wang, W.; Zhang, Y.; Zhang, J.; Li, D.; Leng, D.; Gao, Y.; Gao, J.; Lu, H.; Li, X. Metal−organic framework-derived Cu_2O−CuO octahedrons for sensitive and selective detection of ppb-level NO_2 at room temperature. *Sens. Actuators, B* **2021**, *328*, No. 129045.
(41) Güy, N.; Atacan, K.; Özacar, M. Rational Construction of p-n-p CuO/CdS/$CoWO_4$ S-scheme Heterojunction with Influential Separation and Directional Transfer of Interfacial Photocarriers for Boosted Photocatalytic H_2 Evolution. *Renewable Energy* **2022**, *195*, 107−120.
(42) Li, F.; Gao, X.; Wang, R.; Zhang, T.; Lu, G. Study on TiO_2-SnO_2 Core-Shell Heterostructure Nanofibers with Different Work Function and Its Application in Gas Sensor. *Sens. Actuators, B* **2017**, *248*, 812−819.
(43) Chen, J.; Qin, W.; Li, K.; Feng, L.; Chen, J.; Qiao, H.; Yang, M.; Tian, Z.; Li, X.; Gu, C.; Wang, Y.; Gong, Z.; Yin, S. A High-Sensitivity, Fast-Response and High-Stability Humidity Sensor of Curly Flake $Ti_3C_2T_x$ MXene Prepared by Electrolytic Intercalation of NaOH Solution. *J. Mater. Chem. A* **2022**, *10*, 22278−22288.
(44) Li, N.; Jiang, Y.; Zhou, C.; Xiao, Y.; Meng, B.; Wang, Z.; Huang, D.; Xing, C.; Peng, Z. High-Performance Humidity Sensor Based on Urchin-Like Composite of Ti_3C_2 MXene-Derived TiO_2 Nanowires. *ACS Appl. Mater. Interfaces* **2019**, *11*, 38116−38125.
(45) Zhang, D.; Sun, Y.; Li, P.; Zhang, Y. Facile Fabrication of MoS_2-Modified SnO_2 Hybrid Nanocomposite for Ultrasensitive Humidity Sensing. *ACS Appl. Mater. Interfaces* **2016**, *8*, 14142−14149.

https://doi.org/10.1021/acsomega.2c07098
ACS Omega 2023, 8, 4878−4888